Protective Relaying for Distribution and Microgrids Evolving from Radial to Bi-Directional Power Flow

T. E. McDermott*, T. Smith†, J. Hambrick†, A. Barnes‡, R. Fan*, B. Vyakaranam*, P. Thekkumparambathmana* and Z. Li†
*Pacific Northwest National Laboratory, Richland, WA 99352 USA. Email: Thomas.McDermott@pnnl.gov, Rui.Fan@pnnl.gov, BharatGNVSR.Vyakaranam@pnnl.gov, Priya.Thekkumparambathmana@pnnl.gov
†Oak Ridge National Laboratory, Oak Ridge, TN 37831 USA. Email: smithtm@ornl.gov, hambrickjc@ornl.gov, liz2@ornl.gov
‡Los Alamos National Laboratory, Los Alamos, NM 87545 USA. Email: abarnes@lanl.gov

***Abstract*— As distributed energy resources (DER) achieve higher penetration levels in distribution systems, the normal flow of power (and fault current) is no longer unidirectional, from substation source to load (or fault). The increased importance of DER has also led to revisions in the DER interconnection standards, particularly voltage regulation and ride-through, with publication of a new IEEE Standard 1547-2018. These changes have complicated normal distribution system operation, and they will also complicate distribution system protection. The U. S. Department of Energy undertook a review of protection state-of-the-art for this new environment in order to identify gaps and propose near-term solutions.**

NOMENCLATURE

ACSR	Aluminum cable, steel reinforced
ATP	Alternative Transients Program
c	Speed of light in vacuum
d	Distance
CHP	Combined heat and power
COMTRADE	Common format for transient data exchange
CN	Concentric neutral cable
CT	Current transformer
DER	Distributed Energy Resource
DST	Discrete S transform
I_a	Phase A current
$I_{a\Delta}$	Phase A delta current
LCL	Filter with two inductors, one shunt capacitor
LFG	Landfill gas
LLF	Line-to-line fault
NWP	Network protector
PCC	Point of common coupling
PI	Proportional-integral controller
PLL	Phase-locked loop
PR	Proportional-resonant controller
PV	Photovoltaic
R_1	Positive sequence resistance
R_0	Zero sequence resistance
RCA	Relay characteristic angle
RMS	Root mean square
SLGF	Single line-to-ground fault
SNL	Secondary network load
τ	Wave travel time
TACS	Transient analysis of control systems, in ATP
TRL	Technology Readiness Level
TS	Tape shield cable
UV	Undervoltage trip functions
v	Traveling wave velocity
v_1	Positive sequence wave velocity
v_0	Zero sequence wave velocity
V	Voltage
V_a	Phase A voltage
$V_{a\Delta}$	Phase A delta voltage
V_{op}	Operating quantity
V_{ref}	Reference quantity
VT	Voltage transformer
X_1	Positive sequence reactance
X_0	Zero sequence reactance
Z_c	Characteristic impedance
Z_1	Positive sequence characteristic impedance
Z_0	Zero sequence characteristic impedance
Z_{HSD}	Zone impedance for high-speed detection

I. INTRODUCTION

THIS paper summarizes the state-of-the art for protecting radial distribution feeders, secondary networks, and microgrids with high penetration of DER. Undervoltage trip settings have provided de facto fault detection for DER on many systems, but this will be less effective as the trip times increase under the new IEEE 1547. On secondary networks, a de minimus principle has kept DER from interfering with existing network protectors, but this often limits DER capacity to just a few percent of the serving network transformer capacity. Inverter-coupled DER (e.g., solar, storage) produces low fault current, which often doesn't operate overcurrent devices. Furthermore, the inverter controls (e.g., phase-locked loop) quickly change the inverter current's phase angle during a fault, so that it doesn't lag the inverter voltage during faults the same way as with conventional DER. As a result, directional and distance relays may not perform as expected with inverter-based DER. Differential protection schemes have been successful on transmission systems, but the many taps and loads found on distribution systems make it difficult to apply differential protection. Furthermore, the expense of protection-

grade communications (e.g., direct transfer trip) has been a barrier to some DER projects. Even when communication infrastructure for metering has been installed, it often does not meet the speed and reliability requirements for protection.

Near-term solutions are necessary to cope with the new IEEE 1547 [1]. The paper focuses on schemes that have been successful elsewhere (e.g., transmission) and for which commercial products exist, even if they haven't been applied on distribution before. Extensive communication system upgrades have been ruled out for the near term. To evaluate schemes, an 11-point set of metrics was applied to electromagnetic transient simulations of IEEE distribution test feeders, with some extensions, in ATP or MATLAB SimScape Power Systems, followed by relay simulations in Mathcad or Simulink. For radial systems, the schemes included focused directional, single-point traveling wave, and incremental distance relays. For secondary networks, the schemes included a cut-set differential and some changes to the network protector relay. For microgrids, the schemes included differential *S*-transform and admittance relays. Each scheme can be successful in some circumstances.

A. Summary of Changes to IEEE Std. 1547

IEEE 1547-2018 defines two categories of DER for voltage regulation and reactive power control:

- Category A – minimum performance
- Category B – for high penetration scenarios

and three categories for response to disturbances:

- Category I – essential needs of the bulk power system
- Category II – ride-through compatible
- Category III – for high penetration scenarios

As in earlier versions, the new standard states requirements that DER cease to energize the utility power system and trip during faults. "Cease to energize" means no active power delivery, but in the new version, limited reactive power exchange is allowed. This reactive power limit is 3% or 10% of nameplate, depending on size, and must only come from passive devices that serve the DER. During ride-through scenarios, the DER may provide dynamic reactive power for voltage support. As in earlier versions, the DER must coordinate with utility ground fault protection and automatic reclosing practices but "cease to energize" (i.e., no trip) meets the coordination requirement for reclosing. For unintended islands, the default time to detect and cease to energize is still 2.0 seconds, but the new standard allows adjustability up to 5.0 seconds. These are all functional requirements, and not explicitly linked to UV trip settings.

Table I summarizes the UV trip settings in different versions of IEEE 1547 (Note: UV numbers were not used before 2018, but Table I adopts the 2018 numbering scheme for earlier versions in order to facilitate comparisons). The UV2 function has often been used as de facto fault detection, or backup fault detection, especially for inverter-based DER. For Category III DER, in high penetration scenarios, the default UV2 trip time has increased from 0.16 to 2.00 seconds, and may be adjusted up to 21.0 seconds. This impairs the de facto use of UV2 for fault detection. Other complicating factors may include the increase in islanding detection time, and the allowance for dynamic reactive power during voltage disturbances.

TABLE I. Undervoltage Trip Settings in IEEE Std 1547

Description	Default		Maximum	
	V [pu]	Time [s]	V [pu]	Time [s]
1547-2003 UV1	0.88	2.00	n/a	n/a
1547-2003 UV2	0.50	0.16	n/a	n/a
1547-2014a UV1	0.88	2.00	n/a	21.0
1547-2014a UV2	0.60	1.00	n/a	11.0
1547-2014a UV3	0.45	0.16	n/a	1.0
1547-2018 Cat I UV1	0.70	2.00	0.88	21.0
1547-2018 Cat I UV2	0.45	0.16	0.50	2.0
1547-2018 Cat II UV1	0.70	10.00	0.88	21.0
1547-2018 Cat II UV2	0.45	0.16	0.50	2.0
1547-2018 Cat III UV1	0.88	21.0	0.88	50.0
1547-2018 Cat III UV2	0.50	2.00	0.50	21.0

B. Broader Landscape of DER Protection

Over the next one to five years, increasing penetration of DER and microgrids will create new protection challenges in several areas beyond those posed by IEEE Std. 1547-2018.

Mixtures of rotating machine and inverter-based DER will complicate the detection of unintentional islands [2]. Rotating machines can look too much like the utility grid for the built-in inverter islanding detection methods to work properly. These are currently tested only for single inverters connected to the grid. A realistic scenario with many inverters of different make and size would also be difficult for islanding detection, as the built-in algorithms can work against each other. For example, inverter A tries to move the grid frequency upward while inverter B tries to move the frequency downward. The end result could be that the grid frequency doesn't shift, so the island isn't detected.

Inverter-based DER acts like a voltage-controlled positive-sequence current source, with little or no zero sequence and negative sequence content. Rotating machines in DER act like voltage sources, much like the grid itself. The behavior of rotating machines on the grid is well understood; simplified fault current models are available, with dynamic and transient models also available if needed. The rotating models, software tools, and machine type tests, which are the basis for model parameters, have evolved together over more than 100 years of operating experience. Inverters are much newer and much different than rotating machines; they don't provide much fault current, they can follow the terminal voltage angle very quickly, and there are no standard type tests for simplified fault models. This makes it harder to perform protection analysis and increases the chance for errors.

Microgrids can operate in and transition between different modes, including grid-connected, intentionally islanded after separating from the grid, and black start (sometimes called grid forming). Each mode calls for different control responses to maintain voltage and frequency. The available fault current magnitudes and directions also change significantly between modes. In a normal utility protection study, the fault currents at a given location change with different system configurations, but usually within a range of two-to-one. With relatively few exceptions, one relay scheme and one relay settings group works well for each location. This isn't true for microgrids

because the strengths and types of sources vary much more, so the protection schemes and settings need to be more adaptive.

Overcurrent relays only need CT sensor inputs, but directional overcurrent relays also need VT inputs to determine phase angle (i.e., direction) of the current with respect to voltage. VTs are also needed for distance relays and many other types of protection. If the voltage drops too low during a fault, the VT output can be too low for the phase angle determination, which leads to loss of directionality. This can be mitigated inside the substation, but it's harder to deal with out on the feeder, including at DER locations. This is one example of how new relaying schemes could increase the requirements on distribution system sensors.

For the longer term, there are more significant gaps to be addressed. These include cost-effective sensors and communication channels for advanced protection schemes on distribution. Precision timing and cyber security must be provided. New type tests and fault models for inverter-based DER are also required to efficiently complete protection studies.

II. Objectives

The top-level objective is to identify promising state-of-the-art solutions for protective relaying in a bi-directional power flow environment at the distribution and microgrid levels, leading to possible field trials. When a utility engineer designs the protection for a distribution system, the devices, algorithms, and settings are specified to achieve the goals of "dependability, security, sensitivity, and speed". Cost might be included as a metric, but it's not usually a major factor when the communications infrastructure is already in place. There are lists of preferred vendors and relays, and the cost of protection is a small percentage of total system cost. However, in proposing brand new protection schemes, cost must be included along with the basic protection metrics. Any new workforce training requirements would also be included in the cost. Engineers might have to write and test custom programs for digital relays, which would also be a cost.

In the context of a research effort aimed at solving bi-directional power flow issues in the near term, two additional metrics become important. First, flexibility should be considered, as any new protection scheme should allow more bi-directional power flow on the distribution system. Second, technological maturity should be considered, as we need to choose functions that are available in commercial products or could be quickly developed.

Table II summarizes and categorizes the quantitative evaluation metrics for use in evaluating new protection schemes. The first three, indicated with red highlights, are considered essential. The others are used for ranking.

TABLE II. Scheme Evaluation Metrics

Metric	Category	Description
1	Dependability	Must detect all faults within the protected zone; failures are disqualifying
2	Security	Must not trip for any fault outside the protected zone; failures are disqualifying
3	Selectivity	Must trip the minimum number of devices to isolate the fault, after any reclosing activity has completed. Primary protection must trip before backup protection. Failures are disqualifying.
4	Sensitivity	Maximum ground fault resistance before the scheme fails to operate for a ground fault. This can be presented in the form of a graph of resistance vs. fault location.
5	Speed	Time between fault inception and a relay command to trip. This can be presented in the form of a graph of time vs. fault location for different types of fault.
6	Cost	Expected purchase, design, and installation costs for all relays and sensors, per feeder, including both utility-owned and DER relays for a high-penetration case.
7	Cost	Expected purchase, design, and installation costs for new communications infrastructure, per feeder, to support the new scheme. Significant communication costs are disqualifying for now.
8	Cost	Expected training and engineering costs for a new scheme, per utility, consulting, or DER organization.
9	Flexibility	The highest DER penetration level, defined as DER Capacity / Peak Load, for which no disqualifying failures occur.
10	Maturity	The TRL of commercial products that could implement the new scheme.
11	Maturity	The number of vendors that currently supply products that could implement the scheme.

III. Methods

For this paper, protection schemes are analyzed with the aid of software models and simulations. The model files will be made available to licensed users of the respective simulation tools, none of which are open source, through a mechanism still to be determined.

A. System and Relay Modeling

Protection schemes for radial feeders and secondary networks were assessed using an electromagnetic transient simulation program called ATP, and a general modeling program called Mathcad [3]. The IEEE 13-bus [4] and (eventually) 8500-node [5] radial test feeders are modeled in ATP, which then simulates current and voltage waveforms during a variety of system conditions and fault events. The IEEE test feeders are publicly documented and widely used by researchers, which fosters replicability of the results presented later. Once the model has been built, ATP can be scripted for efficient parameter sensitivity studies. ATP exports the waveforms in COMTRADE format, which is one of the formats used for open-loop hardware testing of relays [6]. Therefore, the approach and models presented in this report can be adopted later for laboratory testing.

Fig. 1 shows the ATP model of an IEEE 13-bus system, used to evaluate the incremental and focused directional functions. This system is unbalanced, with a mixture of 3-phase, 2-phase, and 1-phase lines and loads. In converting the data from power flow simulation to transient simulation, all loads were made constant impedance, and the substation transformer taps were fixed to maintain acceptable voltage under peak load. The lines were modeled with frequency-dependent, traveling-wave

components instead of lumped impedances. These changes were appropriate and necessary because the original power flow data emphasizes non-linear load behavior and transformer tap changes over long time frames, while the ATP data emphasizes high-frequency behavior over very short time frames.

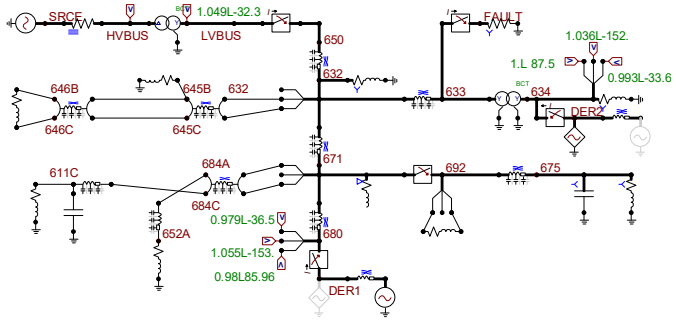

Fig. 1. IEEE 13-bus feeder with DER1 (Thevenin) and DER2 (Norton).

Fig. 2 shows a version of the 13-bus model for single-point traveling wave simulation, with many of the branches and most of the loads removed. The same fault is applied at time zero of the simulation, with a time step of 1 ns, and the simulation ends at 40-200 μs. The simulation time is short to capture the traveling wave arrivals and reflections caused by the fault; it is not intended to capture the peak fault current.

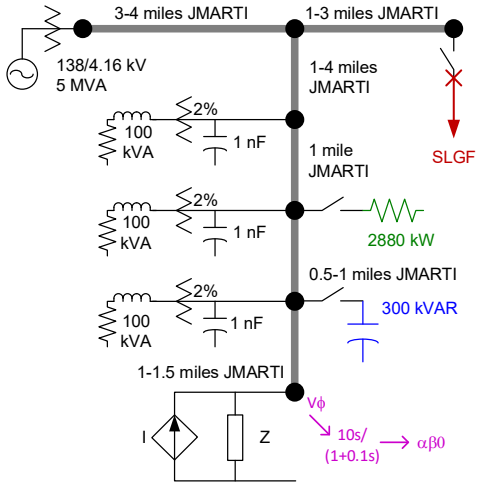

Fig. 2. Traveling wave line and transformer models.

Fig. 2 also shows in magenta how the voltage signals are processed through a low-pass filter, differentiator, and Clarke transformation to assist in detecting wave arrival times [7]. That processing was part of the ATP model for this paper, but it could also be done after simulation. The voltage sensor design is important, because most available VTs don't have adequate frequency response. The use of CTs has been suggested in order to use current waves instead of voltage waves, but the resulting wave signatures are not as easy to identify [7]. A capacitive voltage sensor has also been suggested, with a secondary current sensor connected at the grounded end of the capacitance. This kind of sensor would have adequate frequency response, but it represents an extra cost [8].

B. DER Modeling

Rotating machine DER includes traditional backup gensets, CHP, LFG, small hydro, and older wind turbine generators of types 1-3. A rotating machine is represented with a voltage source behind impedance, or Thevenin equivalent (Fig. 3 left), and it provides 5-6 times rated current to a fault on its terminals. During a fault, the phase relationship between terminal voltage and current can change suddenly because the Thevenin source angle doesn't change very much, due to inertia and the relatively slow machine excitation controls. On a radial distribution feeder, such DER behaves similarly to the substation source, but is not as strong.

Inverter-based DER includes primarily solar photovoltaic (PV) and batteries, but also newer wind turbine generators of type 4, and fuel cells. These are represented with a voltage-controlled current source in parallel with an impedance, or Norton equivalent (Fig. 3 right). Fast-acting inverter controls limit the fault contribution to no more than 2 times rated current, and usually no more than 1.1 times rated current. The inverter controls may also act quickly to hold a constant phase angle between current and voltage, so the source angle can change quickly. On a radial distribution feeder, such DER provide little fault current on their own, although certain types of interconnection transformer may contribute significant ground fault current.

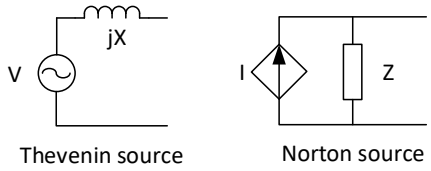

Fig. 3. Controlled current source (Norton equivalent) for inverter-based DER, and Thevenin equivalent voltage source for rotating machine DER.

The inverter model was developed to mimic the behavior of a real single-phase inverter, in simplified form. First, block diagram logic was implemented to maintain real power output at the steady-state value, subject to a limit on the RMS value. Because of this, under low-voltage conditions the inverter current increased to a limit of around 1.1 per-unit. Second, a PLL was implemented using a quarter-cycle transport delay for single-phase inverters [9]. After any disturbance, the PLL acted to bring the output voltage and current in back in phase. This also had the side effect of appearing to control reactive power, but that was not the PLL's main purpose. We only wanted to obtain realistic results for the dynamic angle behaviors during fault conditions. A real PLL would provide the same function, but perform differently. The logic for both magnitude control and PLL were used to drive a controlled current source component in ATP.

Fig. 4 shows the phase A voltage (green) and current (blue) for DER, during a LLF, as represented by Thevenin (left) and controlled Norton (right) sources. In both cases, the pre-fault current and voltage are in phase, the fault occurs at about 0.167 seconds, and the post-fault voltage is about 0.46 per-unit. The Thevenin source current, representative of a rotating machine, increases to about 6 per-unit, and the current lags the voltage by nearly 90 degrees. The controlled Norton source current, representative of an inverter, increases to about 1.1 per-unit. The current lags the voltage for only one and a half cycles and by less than 90 degrees. After that, the PLL brings the voltage

and current back in phase. The LLF response in Fig. 4 has greater initial phase shift than the more common SLGF.

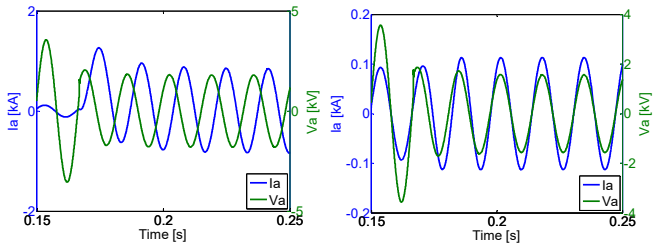

Fig. 4. Thevenin source (left) and Norton source (right) LLF response.

IV. Distance and Directional Relays

See Fig. 1 for the DER and fault locations used to evaluate distance and directional schemes on radial feeders. Fig. 5 shows the impedance plot at DER1, for both Thevenin and Norton source assumptions, during a SLGF on phase A. This is a polar plot, with reactance, *jX*, on the vertical axis and resistance, *R*, on the horizontal axis, both in Ohms. The positive sequence line impedance from DER1 to the substation is about 0.94 + j 3.00 Ohms, plotted as a blue line. Zone 1, the green circle, is set for 80% of the line impedance and Zone 2, the brown circle, is set for 150% of the line impedance. The complex ratio between voltage and current is plotted as a red line, and it migrates from a normal loading condition towards the origin. Each sample impedance is marked with a red X.

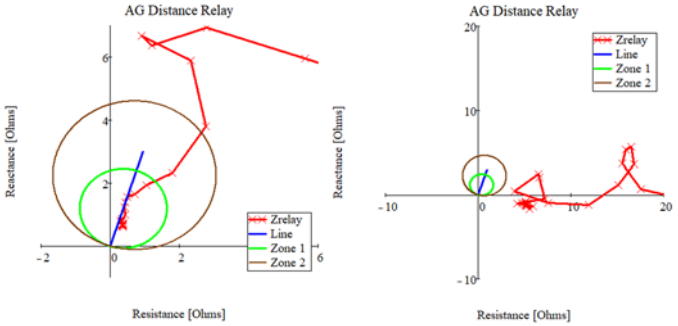

Fig. 5. DER1 distance relay with Thevenin (left) and Norton (right) sources.

On the left-hand plot, for a Thevenin source, the starting impedance location has been cropped at the right-hand edge, but after the fault, it moves close to the blue line, and well within Zone 1. One might expect the post-fault impedance to settle near 0.86 + j 2.18 Ohms, which is the positive sequence impedance of the 3500 feet of line directly between DER1 and the fault location. The observed fault impedance is less than half that value, due to the effects of tapped loads.

On the right-hand plot, for a Norton source, the starting impedance is resistive, with a value of about 32 Ohms. During the fault, this impedance migrates towards the origin, and settles at a value of about 4 Ohms, primarily resistive. This value does not lie within either Zone 1 or Zone 2, so a distance relay set to cover the line between DER1 and the substation would not trip.

Memory-based incremental quantities [8, 10] can produce a useful operating quantity for both Thevenin and Norton DER, see equations (1) and (2):

$$V_{ref} = V_a - |Z_{HSD}| I_a \quad (1)$$

$$V_{op} = -V_{a\Delta} + |Z_{HSD}| I_{a\Delta} \quad (2)$$

Fig. 6 shows the phase A voltage and current waveforms for a SLGF occurring at 10 cycles, under conditions similar to those in Fig. 5 (right). Compared to the LLF in Fig. 4 (right), there is very little initial phase shift in the current. In Fig. 7, delta signals are created from differences between the instantaneous voltage and current values, and their instantaneous values one cycle earlier. The first few cycles of delta signal are non-zero while a digital filter initializes, but then they settle to near zero values in steady-state, as expected. After the fault occurs at 10 cycles, both voltage and current waveforms deviate from their pre-fault values, and this creates non-zero delta signals. Fig. 8 shows the operating and restraint quantities from equations (1) and (2). There are two cycles of operating quantity exceeding the restraint quantity, so a trip decision could be made quickly. However, the delta signals return to zero in a post-fault steady state, so a backup method of protection is essential.

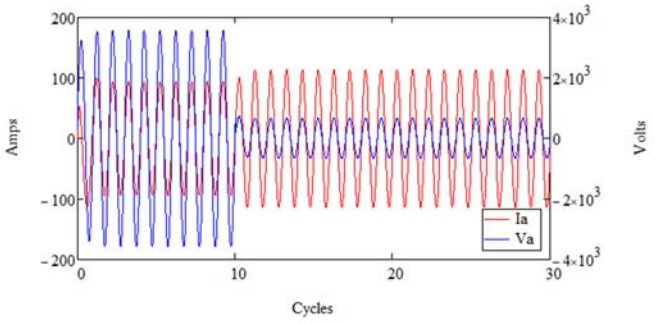

Fig. 6. Distance relay voltage and current response to SLGF with Norton DER.

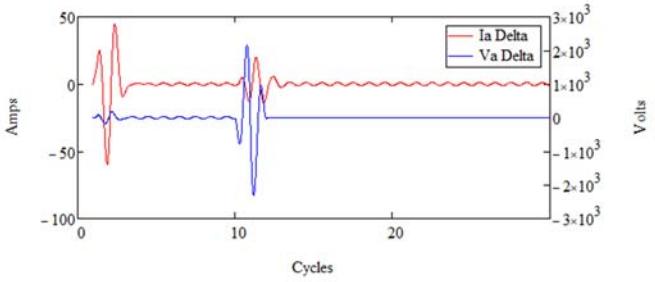

Fig. 7. Incremental distance delta quantities during initialization and SLGF.

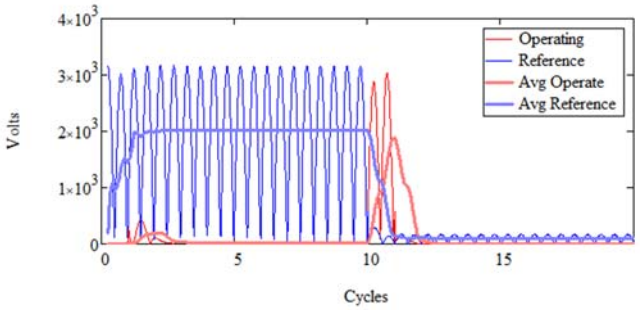

Fig. 8. Incremental distance operating and restraint quantities.

Directional overcurrent relaying (Device Number 67) refers to relaying that determines the direction to fault by comparing the phase angle relationship of phase currents to phase voltages [11]. The relay makes its directional decision by determining if

the angle between the operating current and polarizing voltage has entered the element's operating sector.

The Relay Characteristic Angle (RCA) setting is used in 'Phase angle' Operation mode [12]. A 360-degree setting range is used to represent the settings of angle difference between the operating current phasor (at maximum relay torque) with respect to the polarizing voltage (reference), as shown in Fig. 9. Because the angles between the operating current and polarizing voltage are different for the normal operation and fault conditions, the 360-degree plane could be separated into several operating or non-operating areas by setting proper limits for the minimum and maximum forward and reverse angle.

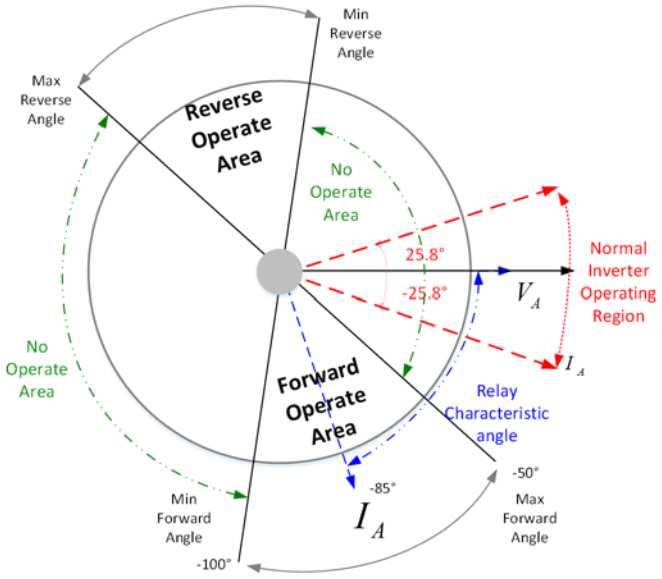

Fig. 9. Focused directional characteristic with inverter operating range.

The operating area for this directional relaying can be "focused" to a certain range, thus the relay will only operate when the phase current angle (compared to the phase voltage angle) falls into the focused area. That's why this scheme is called "focused directional relaying".

Fig. 10 shows the impedance magnitude and angle response at location DER1 for a SLGF, with either Thevenin or Norton DER source characteristics. In both cases, the pre-fault impedance angle starts near 0 degrees, because the DER injects power near unity power factor. This means pre-fault current is approximately in phase with pre-fault voltage. During the fault with Thevenin DER source characteristics, the impedance angle shifts close to +60 degrees. This corresponds to a current angle of approximately -60 degrees, which maps well into the Forward Operate Area of Fig. 10. However, with Norton DER source characteristics, the post-fault impedance angle settles to a value close to zero degrees. This corresponds to a current angle of zero degrees, in the Normal Inverter Operating Region of Fig. 10, so the focused directional relay would not operate.

The focused directional relay works for conventional rotating machines, but not for the ideal inverter Norton source models considered here. In Fig. 9, the normal inverter operating region lies within the relay's no operate area. It's assumed that the inverter control will act quickly to maintain the current angle close to the pre-fault condition, which defeats the angle change that a focused directional scheme relies on. Time delay in the inverter response might compensate for this. For example, angle-tracking might be delayed for two or three cycles, giving the relay time to operate. Incremental distance relaying, presented earlier in this section, is one example.

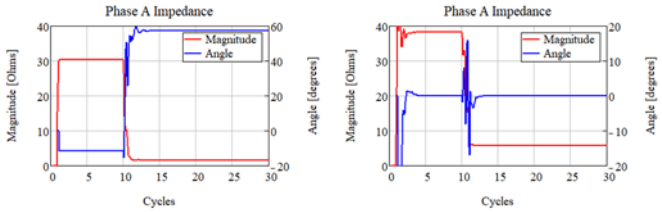

Fig. 10. DER directional with Thevenin (left) and Norton (right).

This analysis of focused directional relaying is based on the inverter behavior. Certain types of interconnection transformer, if they present a ground source to the feeder primary, would modify this behavior for ground faults (only). A ground focused directional relay may be considered for use with inverters, to operate on the ground or zero sequence current. However, a ground relay would not be expected to operate for line-to-line or three-phase faults, so we did not analyze it further.

V. Traveling Wave Relays

Reference [7] describes the basics of single-point and double-point traveling wave protection for transmission lines. Fig. 11 defines the main parameters of the scheme used in this analysis. When a fault occurs, the voltage suddenly drops toward zero, and the current suddenly increases. These voltage and current waves travel outward to other parts of the system, which don't "know" that a fault has occurred, nor what the ultimate fault current magnitude will be, until the traveling wave propagations have settled to a new steady state condition. Each time the waves encounter a circuit branch, load, or generator, there are reflections and transmissions (i.e., refractions) that alter the wave characteristics.

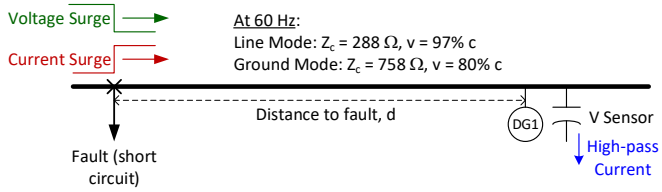

Fig. 11. Constant-parameter model of traveling wave fault detection.

A traveling wave protection scheme identifies the fault by signatures in the arriving current and/or voltage waves. It estimates the fault location by differences in arrival times between various traveling waves. Conventional relays operate on signals that are measured over a time frame of cycles or seconds. Traveling wave relays operate on signals that are measured over a time frame of microseconds. The sensors and processing logic must be faster in traveling wave relays.

As indicated in Fig. 11, the waves travel at speeds approaching the speed of light, c, which is 300 m/μs, or approximately 1000 ft/μs. There is an equivalence between distance, d, and wave travel time, τ, in which $\tau = d/v$, where v is the wave velocity in the same units of length (per time) as d.

For example, it takes about 5 μs for a wave to travel down 5000 feet of overhead distribution line.

On three-phase lines, there are three modes of traveling wave propagation. In the constant-parameter approximation (e.g., the "KC Lee" model in ATP), each one has a different velocity. For overhead lines, two of these are line modes with velocity close to the speed of light, and characteristic impedance, Z_c, in the range of 250 – 400 Ohms. These are analogous to the line's positive sequence and negative sequence impedances. Z_c is the instantaneous ratio between traveling voltage and current waves, and it's primarily resistive. An overhead line also has a ground mode, corresponding to the zero sequence, with Z_c significantly higher than the line modes, and with v significantly lower than the line modes.

Reference [7] suggested that the ground mode not be used for double-ended schemes, because of its higher distortion and attenuation compared to the line mode. In contrast, this analysis considers the difference in arrival times between the line and ground mode waves in a single-ended scheme, also suggested in [7]. The transmission line traveling wave relays can assume there are no taps within the protected line, but on distribution lines, there will be many such taps that distort the waves. This distortion will complicate signature identification, and also the decomposition of waves into arriving, reflecting, and refracting components [7]. This is partially mitigated by the shorter line lengths found on distribution systems compared to transmission systems. The farther the wave travels, the more it attenuates and distorts.

Table III summarizes the sequence impedance and traveling wave parameters for the line construction types used in the IEEE 13-bus test circuit. These are based on the line physical spacing and conductor characteristics, which produce resistance, inductance and capacitance parameter matrices for the line at 60 Hz [4]. These are converted to constant traveling wave parameters according to equation (3), applied separately for positive and zero sequence:

$$Z_c = \sqrt{L'/C'} \qquad v = 1/\sqrt{L'C'} \tag{3}$$

Where L' and C' are the positive sequence or zero sequence inductance and capacitance, respectively, per unit length. For example, L' in Henries per mile and C' in Farads per mile would yield Z_c in Ohms and v in miles per second. In Table III, the v values are normalized to percent of the speed of light. The line capacitance values are often ignored in distribution power flow calculations, but they are essential to determine the traveling wave parameters.

TABLE III. Line Parameters of 13-Bus Test Circuit [4]

#	Type	R_1	X_1	R_0	X_0	Z_1	v_1	Z_0	v_0
	Units	Ω/mi	Ω/mi	Ω/mi	Ω/mi	Ω	%c	Ω	%c
601	3ϕ 556	0.188	0.600	0.660	1.908	288	97.15	758	80.37
602	3ϕ 4/0	0.592	0.762	1.065	2.071	342	90.70	809	79.02
603	2ϕ 1/0	1.120	0.893	1.746	2.285	400	90.52	889	78.70
605	1ϕ 1/0			1.332	1.353			547	81.78
606	3ϕ CN	0.489	0.412	1.407	0.451	53.4	26.20	55.8	25.05
607	1ϕ TS			1.386	1.390			122	17.73

Given Z_c and v, we can determine L' and C' using equation (4), applied separately for positive and zero sequence:

$$L' = Z_c/v \qquad C' = 1/Z_c v \tag{4}$$

where L' and C' will be in Henries and Farads, respectively, per unit length consistent with the units of v. If given in percentage of c, then v should be converted to some physical unit of length per second. Equation (4) can be helpful in estimating C' when that value is not available, because L' is usually available, and reasonable defaults may be estimated for Z_c and v based on the type of line.

In Fig. 12, the power-invariant Clarke transformation has been applied to separate the individual phase signals into alpha and zero components, which correspond to a line mode and the ground mode, respectively. The Clarke transformation is an alternative to symmetrical components, and it's often used for real-time applications because it doesn't require the use of complex numbers. Equation (5) defines the voltage transform.

$$\begin{bmatrix} V_\alpha \\ V_\beta \\ V_0 \end{bmatrix} = \begin{bmatrix} \sqrt{2/3} & -\sqrt{1/6} & -\sqrt{1/6} \\ 0 & \sqrt{1/2} & -\sqrt{1/2} \\ \sqrt{1/3} & \sqrt{1/3} & \sqrt{1/3} \end{bmatrix} \begin{bmatrix} V_a \\ V_b \\ V_c \end{bmatrix} \tag{5}$$

The constant-parameter model is helpful for conceptual analysis, but frequency-dependent line modeling is important to simulate realistic waveforms. There are several formulations for overhead distribution lines, and we chose J. Marti's model for this paper [13]. A frequency-dependent model is always based on physical conductor and spacing data, with values from Table III then calculated over a range of frequencies. Ideally, both alpha and zero modes arrive at the same time because they both travel at near the speed of light. They don't reach peak at the same time because of the frequency-dependent differences in attenuation and distortion. The resulting simulated ground mode will have a delayed peak compared to the line modes, which can be interpreted as a slower velocity. This makes it possible to apply the single-end method to these frequency-dependent waveforms.

In Fig. 12, the decomposition of frequency-dependent waveforms produces different apparent arrival times for alpha (blue) and zero (green) mode waves, measured as time delays between peaks. Fig. 12 indicates both peaks with red brush marks, and the time difference between them is 7.78 μs. Using the data from Table III, we estimate 6.75 miles from DER to the fault using equation (6) for line code 601:

$$d = \Delta\tau / \left(1/v_0 - 1/v_1\right) = 0.8673\Delta\tau \quad \text{[miles, } \mu\text{s]} \tag{6}$$

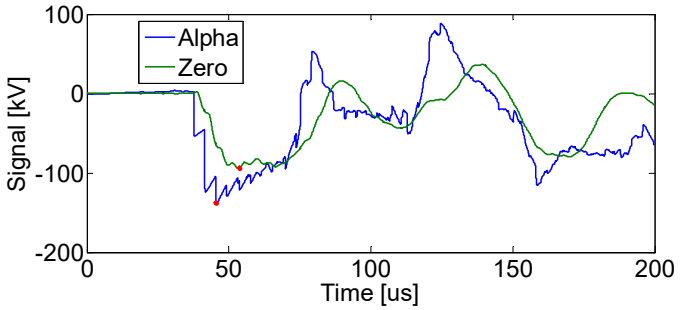

Fig. 12. Alpha and zero component signals for SLGF 7 miles away; the peaks marked in red occur 7.78 μs apart.

This estimate can be improved with weighted values for v_0 and v_1, reflecting changes in line construction between DER and fault location, but the distance error is only 3.6%.

We considered other common events on the distribution system, including load switching and capacitor bank switching, which also produce traveling wave disturbances. The result for the capacitor switching case is provided in Fig. 13. The distance from DER to capacitor bank was estimated at 1.509 miles from the difference, τ, of 1.67 μs between the alpha and zero mode signal peaks. This is close to the actual distance of 1.5 miles.

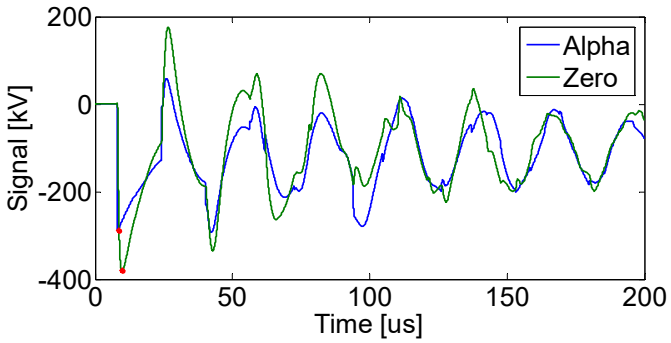

Fig. 13. Alpha and zero component signals for cap switching 1.5 miles away; the peaks marked in red occur 1.67 μs apart.

The single-point traveling wave method shows promise, particularly because unlike the distance and directional schemes, it seems agnostic to the difference between Thevenin and Norton DER sources. Most faults and switching operations (even "closing into chains") will begin on a single phase, and if the event stays single-phase for some tens of microseconds, the generated traveling waves should have separable alpha and zero components during that period. This is long enough to operate the relay, but a different backup scheme would be needed.

There are several open points to investigate before planning field trials of a single-point traveling wave method on radial distribution feeders. These are planned for future work:

1. Add dozens of branches and hundreds of load-serving transformers to the model structure in Fig. 2. This would be typical of a real feeder, and is expected to limit the method's sensitivity.
2. Catalog the expected signatures for all fault types. These have to be differentiated from other events, like load switching, capacitor switching, and tap changes, which also produce traveling waves.
3. Explore alternative traveling wave-based methods for three-phase cables and single-phase lines, which might not have readily separable alpha and zero modes.
4. Perform scripted analysis of more fault types, fault resistance values, DER sizes and locations, single-phase and two-phase fault locations, and underground vs. overhead systems to apply the metrics in Table II.

The requirement of using a capacitive voltage sensor is also a cost issue. Digital filtering on the PCC voltage might provide an equivalent signal, but only if the PCC voltage sensor has adequate frequency response and the digital filter operates fast enough. The relay must be able to resolve time differences of 0.1 to 1.0 μs.

The relay must detect and operate on the very first wave arrival. After that, wave reflections and refractions from other components in the system would probably make the relay insecure from false operations. This means that a traveling wave relay could fill the same role as instantaneous overcurrent relays, which trip immediately when the current is so high that the fault location is certainly nearby. A slower-acting function would have to be provided complementary to the traveling wave function, as time overcurrent relays are comparable to instantaneous overcurrent relays. The single-ended, traveling current wave method suggested recently in [14] could mitigate the need to operate on the first wave arrival. However, the multiple taps and loads on distribution systems could still make this difficult.

VI. Secondary Network Protection

Fig. 14 shows part of a secondary network in a downtown urban area, in which a three-phase 208-Volt grid network is served from six medium-voltage radial feeders. If there is a fault on the low-voltage side, fuses or cable limiters (a type of fuse) will clear it because network protectors (NWP) do not trip for forward power flows. If fuses or cable limiters are not used, the fault may burn clear. Blown fuses and limiters will eventually be replaced, but there is enough redundancy on the low-voltage side that this doesn't have to occur immediately. This improves the service reliability because there are still active cable paths to each SNL, and all of the primary feeders are still in service. If there is a feeder fault on the primary, its breaker opens as usual, while the two NWPs (green) open quickly on reverse power flow. The SNLs experience no interruption in service even after several simultaneous contingencies on either the secondary or primary. The main feature of this design is its high service reliability.

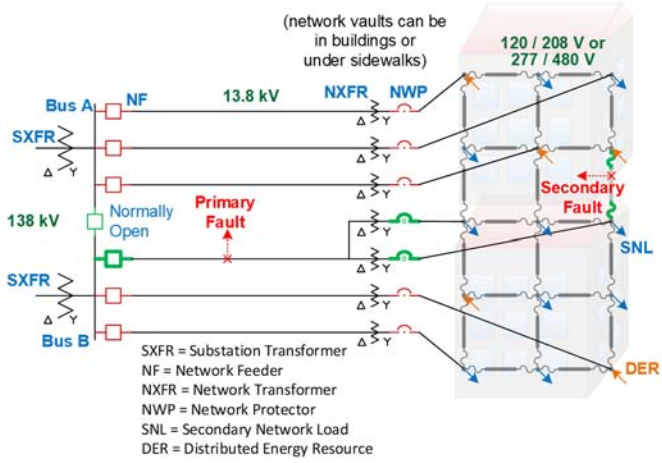

Fig. 14. Secondary network response to primary and secondary faults.

It's an essential feature that the NWP will open on low-magnitude reverse power flow, so that the NWPs open whenever the feeder breaker opens in absence of a fault. This requirement has limited the penetration level of DER connected to such secondary networks. No reverse power flow can be allowed through the NWP during normal operation. Existing practice is to limit DER so that reverse power flow is essentially impossible, either at the building, facility, or network level [15,

16]. This would preclude high-penetration of DER on secondary networks.

By means of ATP simulation, we found that a cut-set differential scheme [17] could work on secondary networks, but it does require communications between the substation and each NWP. The cut-set functions like an extended differential scheme, incorporating lines, transformers, and switchgear. Distance relays were considered looking back into the primary feeder, but many NWP vaults don't have space for the required submersible VT and CT sensors. Some utilities have de-sensitized the NWP relay trip setting in order to accommodate possible reverse power flow from DER. The NWP still trips at current levels representative of multi-phase primary feeder faults but may not trip for the SLGF. Also, if the NWP has to open after the primary feeder opened without a fault, communications is required. Before desensitization, the NWP would have tripped in that situation based just on the reverse supply of transformer magnetizing current and circulating flows through closed NWPs. In all cases, the scheme needs to handle cases where the primary feeder also supplies "regular" load, not just secondary networks. We have not yet identified a state-of-the-art solution that meets all objectives stated earlier.

VII. Microgrid Protection

Microgrids have existed for over a hundred years, and when supplied from local synchronous generation, the protection schemes are well understood. The same principles apply when that kind of microgrid operates in parallel with a single strong utility source. Problems arise when inverter-fed microgrids need to operate either utility-connected or standalone. The disparity in fault current levels between these modes makes it difficult to set overcurrent relays [18]. Recent suggestions have included a supplemental source of fault current for microgrid mode, or directional comparison relaying with cascading time delays [19]. The first idea creates a new single point of failure for the whole protection system, and the second idea produces longer and longer fault clearing times. Both may increase equipment damage until the fault is cleared.

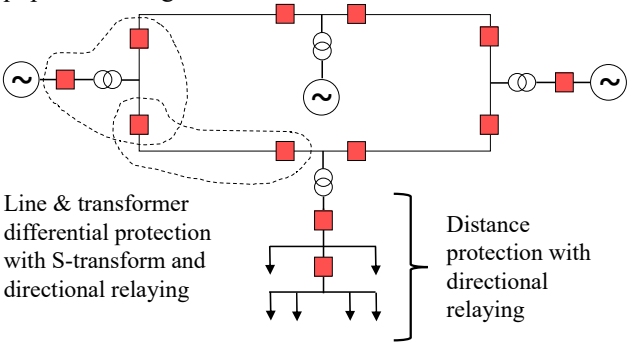

Fig. 15. Proposed microgrid protection schemes.

Two promising alternate protection schemes are evaluated that can operate with or without fault current, the differential *S*-transform method [20] and the admittance (or Mho) method [21, 22]. The *S*-transform is a time-frequency transform that preserves phase information. The discrete version (DST) is used in this study, as given in equation (7):

$$S[j,n]=\sum_{m=0}^{N-1}X[n+m]\exp\frac{-2\pi^2m^2k^2}{\left(a+b\sqrt{|f|}\right)^2}\cdot\exp\frac{\mathbf{i}2\pi mj}{N} \quad (7)$$

where $X[n]$ is the discrete Fourier transform of the signal $x(k)$ in equation (8):

$$X[n]=\frac{1}{N}\sum_{k=0}^{N-1}x[k]\exp\frac{-\mathbf{i}2\pi mk}{N} \quad (8)$$

In the preceding equations (7)-(8) $j = 1,2,\ldots N-1$ is the time index and $n = 0,1,\ldots N-1$ is the frequency index. The energy is defined in equation (9) as:

$$E[j]=\sum_{n=0}^{N-1}\left|S[j,n]\right|^2 \quad (9)$$

For protection, the difference in energy of the *S*-transformed sending and receiving current is used as an operating quantity for tripping. The energy difference is a quantity that is robust against communications transport delay.

The admittance method has the following advantages over the DST method: it does not require communications, paired protection on either end of the protected element, or hardware capable of carrying out time-frequency transforms in real-time. It is also suitable for protecting load buses.

To test the two proposed microgrid schemes, the case study system of Fig. 16 is utilized, with the parameters described in Table IV. This consists of a two-bus microgrid operating in standalone mode while supplied by a grid-forming inverter at bus 1. The inverter operates with a proportional-resonant (PR) controller, as described in [23]. The PR controller has advantages over a proportional-integral (PI) controller in that it does not require converting measured quantities into a rotating reference frame, thereby making it more amenable to implementation on fixed-point controllers, and also is able to compensate for low-order current harmonics.

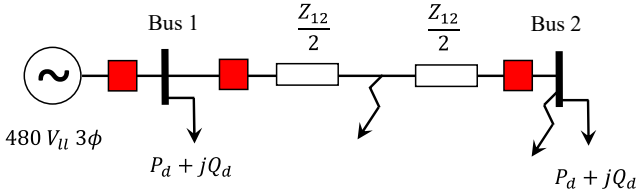

Fig. 16. Microgrid case study system.

TABLE IV. Microgrid Parameters

Parameter	Symbol	Value
Inverter voltage	V_{ll}	480 V
Inverter frequency	f_0	60 Hz
Inverter peak current limit	$\hat{I}_{max}$	300 A
Line resistance	$Re(Z_{12}) = R_{12}$	78 $m\Omega$
Line Reactance	$Im(Z_{12}) = X_{12}$	53.4 $m\Omega$
Load real power	P_d	25 kW
Load reactive power	Q_d	12.5 $kVAR$
Fault resistance	R	0.433 Ω

The modeled inverter has two control loops: an inner current/voltage control loop that regulates the ac voltage on the output LCL filter capacitor and an outer droop/virtual impedance control loop. At the time constants of interest (tens of cycles), only the inner voltage control loop is of interest,

while the outer control loop responds on the order of seconds. As the PR controller operates in a stationary reference frame, it has the disadvantage that the current control reaching the maximum output current will result in output voltage harmonics, and any protection employed will need to be robust against such harmonics.

To test the DST for protection, a pair of simulations was carried out on the Fig. 16 case study system with faults at the midpoint of line 1-2 and at bus 2. The relay is at bus 1, looking to the right to protect line 1-2. It should operate for a fault at the midpoint, but not for the bus 2 fault. Fig. 17 illustrates the decrease in inverter output voltage and the appearance of waveform distortion after 0.25 s, as the inverter goes into current-limiting mode. Fig. 18 illustrates the sending and receiving currents on either end of line 1-2. Fig. 19 shows the resulting differential DST energy for both fault locations. The signal is positive for the midpoint fault (should trip) and oscillatory for the bus 2 fault (should not trip). After averaging, this energy signal can form the basis of a relay operating quantity, by comparison to a threshold.

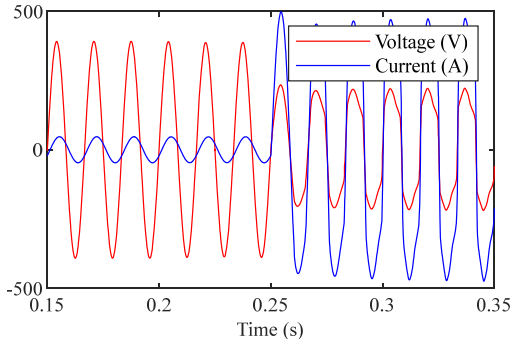

Fig. 17. Voltage and current for a midpoint fault with ¼ cycle delay

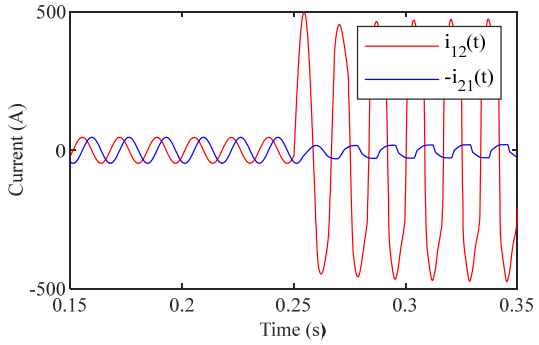

Fig. 18. Sending and receiving currents for a midpoint line-neutral fault with ¼ cycle delay

A limitation of the method is that some ripple is present in the energy on account of the current harmonics, so smoothing is necessary at the cost of response time. An additional issue not demonstrated here is that if two inverters are present on either end of a line so that their fault contributions are identical, the protection will not respond. In such a case, either backup protection is required, such as negative current, zero current, or overcurrent relaying [24], or the method must be extended to add a sign quantity to the differential energy through directional protection. Both of these alternatives carry limitations – the first can result in false trips in the case of severe load imbalance, the second requires the addition of voltage sensing.

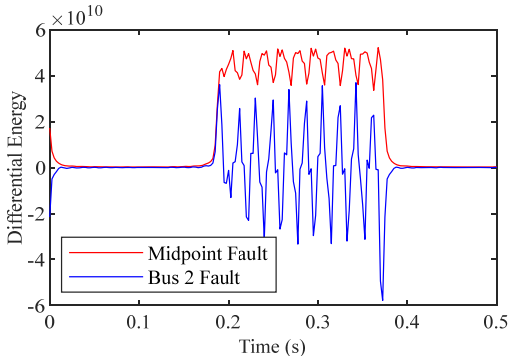

Fig. 19. Discrete S-transform differential energies for line-ground faults with ¼ cycle delay

To test the admittance protection, the same pair of simulations was repeated with the relay at bus 2, looking to the left to protect bus 2. It should operate for the bus 2 fault, but not for the midpoint fault. The results are illustrated in Fig. 20 and Fig. 21. Fig. 20 shows the measured impedance dropping into the trip region, while Fig. 21 shows the impedance drop and then recover. Previous work has documented that admittance protection can result in false trips for upstream line-ground faults [21, 22]. Fig 21 illustrates this behavior occurs briefly in the case study system, and either directional protection or time-delay coordination [25] is needed to overcome this.

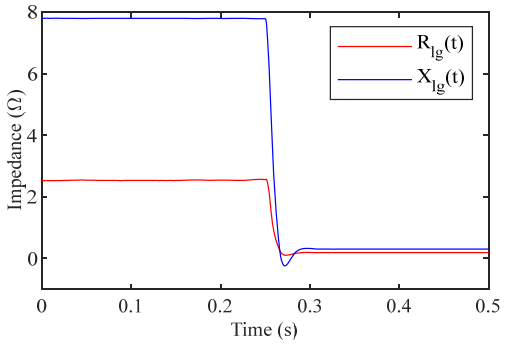

Fig. 20. Line-ground impedance for a bus 2 line-ground fault.

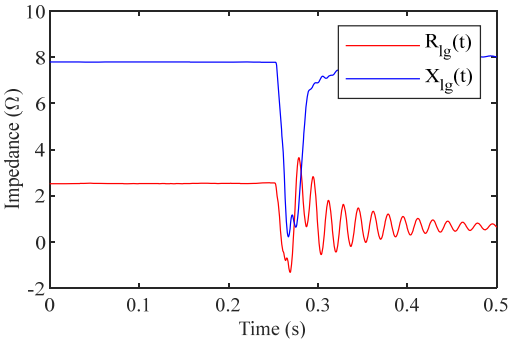

Fig. 21. Line-ground impedance for a midpoint line-ground fault.

VIII. Conclusion

Some promising schemes have been identified for near-term application in high-penetration DER scenarios. For radial feeders, incremental distance, and possibly focused directional or single-point traveling wave could be useful. For microgrids, the discrete *S* transform method has been identified. We don't yet have a good candidate scheme for secondary networks.

The evaluation process for each candidate protection scheme will follow this framework:

1. **Conceptual Design**, which includes literature review, analytical modeling of the power system and protection functions, a peer review by industry protection experts, and outreach to potential demonstration utilities. This produces a candidate protection scheme and test site.
2. **Model-Based Design**, which includes transient or dynamic simulation of event scenarios with relay models in a transient program or a hardware-based simulator. This produces the specifications and settings for relays and sensors.
3. **Hardware Verification**, which includes either open-loop testing or hardware-in-the-loop simulation of the protection scheme at the planned test site. It may be necessary to program utility-grade controllers or microcomputers to implement special algorithms. This step produces a detailed test plan for the demonstration.
4. **Field Trial**, which includes utility installation of the relays and sensors next to the existing protection. The new scheme will detect faults, but not trip. The trial should last at least six months, preferably longer. This step produces a report on verification, performance of the new scheme, and lessons learned.

IX. Acknowledgment

This material is based upon work supported by the U. S. Department of Energy, Office of Electricity Delivery and Energy Reliability. The Pacific Northwest National Laboratory is operated by Battelle for the U.S. Department of Energy under Contract DE-AC05-76RL01830. The Oak Ridge National Laboratory is managed by UT-Battelle, LLC for the U.S. Department of Energy under contract DE-AC05-00OR22725. The Los Alamos National Laboratory is operated by Triad National Security, LLC for the U. S. Department of Energy's National Nuclear Security Administration (NNSA). We are grateful to David R. Smith, PE, for helpful discussions about secondary network operation and protection.

X. References

[1] IEEE, "IEEE Standard for Interconnection and Interoperability of Distributed Energy Resources with Associated Electric Power Systems Interfaces," *IEEE Std 1547-2018 (Revision of IEEE Std 1547-2003),* pp. 1-138, 2018.

[2] L. A. C. Lopes and Y. Zhang, "Islanding Detection Assessment of Multi-Inverter Systems With Active Frequency Drifting Methods," *IEEE Transactions on Power Delivery,* vol. 23, pp. 480-486, 2008.

[3] L. V. Dusang and B. K. Johnson, "Evaluation of fault protection methods using ATP and MathCAD," in *2008 IEEE Canada Electric Power Conference*, 2008, pp. 1-8.

[4] W. H. Kersting, "Radial distribution test feeders," in *2001 IEEE Power Engineering Society Winter Meeting. Conference Proceedings (Cat. No.01CH37194)*, 2001, pp. 908-912 vol.2.

[5] R. F. Arritt and R. C. Dugan, "The IEEE 8500-node test feeder," in *IEEE PES T&D 2010*, 2010, pp. 1-6.

[6] "IEEE/IEC Measuring relays and protection equipment Part 24: Common format for transient data exchange (COMTRADE) for power systems," *IEEE Std C37.111-2013 (IEC 60255-24 Edition 2.0 2013-04),* pp. 1-73, 2013.

[7] E. O. Schweitzer, A. Guzmán, M. V. Mynam, V. Skendzic, B. Kasztenny, and S. Marx, "Locating faults by the traveling waves they launch," in *2014 67th Annual Conference for Protective Relay Engineers*, 2014, pp. 95-110.

[8] E. O. Schweitzer and B. Kasztenny, "Distance Protection: Why Have We Started with a Circle, Does It Matter, and What Else Is Out There?," in *Western Protective Relay Conference*, Spokane, 2017.

[9] R. Teodorescu, M. Liserre, and P. Rodriguez, *Grid Converters for Photovoltaic and Wind Power Systems*: John Wiley & Sons, 2011.

[10] J. Blumschein, C. Dzienis, and M. Kereit, "Directional Comparison based on High-Speed-Distance Protection using Delta Quantities," presented at the Western Protective Relay Conference, Spokane, 2014.

[11] J. Horak, "Directional overcurrent relaying (67) concepts," in *IEEE 59th Annual Conference for Protective Relay Engineers*, 2006.

[12] M. Benitez, J. Xavier, K. Smith, and D. Minshall, "Directional Element Design for Protecting Circuits with Capacitive Fault and Load Currents," in *Annual Western Protective Relay Conference*, Spokane, 2017.

[13] J. R. Marti, "Accurate Modelling of Frequency-Dependent Transmission Lines in Electromagnetic Transient Simulations," *IEEE Transactions on Power Apparatus and Systems,* vol. PAS-101, pp. 147-157, 1982.

[14] A. Guzmán, B. Kasztenny, Y. Tong, and M. V. Mynam, "Accurate and economical traveling-wave fault locating without communications," in *2018 71st Annual Conference for Protective Relay Engineers (CPRE)*, 2018, pp. 1-18.

[15] IEEE, "IEEE Recommended Practice for Interconnecting Distributed Resources with Electric Power Systems Distribution Secondary Networks," *IEEE Std 1547.6-2011,* pp. 1-38, 2011.

[16] A. Bokhari, A. Raza, M. Diaz-Aguiló, F. d. León, D. Czarkowski, R. E. Uosef, *et al.*, "Combined Effect of CVR and DG Penetration in the Voltage Profile of Low-Voltage Secondary Distribution Networks," *IEEE Transactions on Power Delivery,* vol. 31, pp. 286-293, 2016.

[17] P. Mohammadi and S. Mehraeen, "Challenges of PV Integration in Low-Voltage Secondary Networks," *IEEE Transactions on Power Delivery,* vol. 32, pp. 525-535, 2017.

[18] A. R. Haron, A. Mohamed, H. Shareef, and H. Zayandehroodi, "Analysis and solutions of overcurrent protection issues in a microgrid," in *2012 IEEE International Conference on Power and Energy (PECon)*, 2012, pp. 644-649.

[19] N. Hatziargyriou, "Microgrid Protection," in *Microgrids:Architectures and Control*, ed: Wiley-IEEE Press, 2014, p. 344.

[20] S. Kar and S. R. Samantaray, "Time-frequency transform-based differential scheme for microgrid protection," *Transmission Distribution IET Generation,* vol. 8, pp. 310-320, 2014/02// 2014.

[21] J. M. Dewadasa, A. Ghosh, and G. Ledwich, "Distance protection solution for a converter controlled microgrid," 2008.

[22] M. Dewadasa, A. Ghosh, and G. Ledwich, "Line protection in inverter supplied networks," in *2008 Australasian Universities Power Engineering Conference*, 2008, pp. 1-6.

[23] J. C. Vasquez, J. M. Guerrero, M. Savaghebi, J. Eloy-Garcia, and R. Teodorescu, "Modeling, Analysis, and Design of Stationary-Reference-Frame Droop-Controlled Parallel Three-Phase Voltage Source Inverters," *IEEE Transactions on Industrial Electronics,* vol. 60, pp. 1271-1280, 2013.

[24] H. Nikkhajoei and R. H. Lasseter, "Microgrid fault protection based on symmetrical and differential current components," Power System Engineering Research Center2006 2006.

[25] M. Dewadasa, A. Ghosh, and G. Ledwich, "An inverse time admittance relay for fault detection in distribution networks containing DGs," in *TENCON 2009 - 2009 IEEE Region 10 Conference*, 2009, pp. 1-6.